

# An improved catalog of halo wide binary candidates

Christine Allen<sup>1</sup> & Miguel A. Monroy-Rodríguez<sup>1</sup>

*Instituto de Astronomía, Universidad Nacional Autónoma de México, Apdo. Postal 70-264,  
México, D.F. 04510, México; chris@astro.unam.mx*

## ABSTRACT

We present an improved catalog of halo wide binaries, compiled from an extensive literature search. Most of our binaries stem from the common proper motion binary catalogs by Allen et al. (2004), and Chanamé & Gould. (2004) but we have also included binaries from the lists of Ryan (1992) and Zapatero-Osorio & Martin (2004). All binaries were carefully checked and their distances and systemic radial velocities are included, when available. Probable membership to the halo population was tested by means of reduced proper motion diagrams for 251 candidate halo binaries. After eliminating obvious disk binaries we ended up with 211 probable halo binaries, for 150 of which radial velocities are available. We compute galactic orbits for these 150 binaries and calculate the time they spend within the galactic disk. Considering the full sample of 251 candidate halo binaries as well as several subsamples, we find that the distribution of angular separations (or expected major semiaxes) follows a power law  $f(a) \sim a^{-1}$  (Oepik's relation) up to different limits. For the 50 most disk-like binaries, those that spend their entire lives within  $z = \pm 500$  pc, this limit is found to be 19,000 AU (0.09 pc), while for the 50 most halo-like binaries, those that spend on average only 18% of their lives within  $z = \pm 500$  pc, the limit is 63,000 AU (0.31 pc). In a companion paper we employ this catalog to establish limits on the masses of the halo massive perturbers (MACHOs).

*Subject headings:* binaries: general – catalogs – subdwarfs – Galaxy: halo

## 1. Introduction

Old disk and halo binaries are relevant to the understanding of processes of star formation and early dynamical evolution. In particular, the orbital properties of the wide binaries remain unchanged after their formation, except for the effects of the galactic tidal field or of their interaction with perturbing masses encountered during their lifetimes, as they travel in the galactic environment. The widest binaries are quite fragile and easily disrupted by encounters with various

perturbers, be they passing stars, molecular clouds, spiral arms, MACHOs (massive compact halo objects) or the galactic tidal field. In this way, they can be used as probes to establish the properties of such perturbers (Weinberg, Shapiro & Wasserman 1987; Wasserman & Weinberg 1991; Yoo, Chaname & Gould 2004; Jiang & Tremaine 2010)).

An interesting application of halo wide binaries was proposed by Yoo et al. (2004) who used the catalog of Chanamé & Gould (2004, hereinafter ChG) containing 116 halo binaries to try to detect the signature of disruptive effects of MACHOs in their widest binaries. They were able to constrain the masses of such perturbers to  $m < 43 M_{\odot}$ , essentially excluding MACHOs from the galactic halo, since a lower limit of about  $30 M_{\odot}$  is found by other studies (Alfonso et al. 2003; Alcock et al 1998, 2001). However, as was shown a few years later by Quinn et al (2009), this result depends critically on the widest binaries of their sample, as well as on the observed distribution of the angular separations which, according to ChG, shows no discernible cutoff between  $3.5''$  and  $900''$ . Quinn et al (2009) obtained radial velocities for both components of four of the widest binaries in the ChG catalog and found concordant values for three of them, thus establishing their physical nature. The fourth binary turned out to be optical, resulting from the random association of two unrelated stars. Excluding this spurious pair and assuming power law distributions with exponents between 0.8 and 1.6 for the observed separations they find a limit for the masses of the MACHOs of  $m < 500 M_{\odot}$ , much less stringent than that found previously; they conclude rather pessimistically that the currently available wide binary sample is too small to place meaningful constraints on the MACHO masses. They also point out that the density of dark matter encountered by the binaries along their galactic orbits is variable, and that this variation has to be taken into account when calculating constraints on MACHO masses.

Motivated by these concerns, we have constructed a catalog of 251 candidate halo wide binaries. We describe the way the catalog was compiled in Section 2. In Section 3 we present some statistical properties for different subsamples of binaries, and examine the galactic orbits for the 150 binaries with sufficient observational data. Section 4 is devoted to a discussion of our results. We point out that for a total of 9 binaries concordant radial velocities for both components were found in the literature. A companion paper utilizes this catalog to dynamically model the evolution of wide halo binaries, and to obtain new limits on the MACHO masses.

We stress that our study pertains to the wide binaries only. The classical study of Duquennoy & Mayor (1991) and its recent update (Raghavan et al. 2010) shows a log-normal distribution of periods. Our binaries correspond to the periods greater than the maximum period of these distributions, i.e.  $P > 10^5$  yr, which corresponds approximately to semiaxes greater than 100 AU. For our present purpose, we use the term “wide binary” to refer to binaries with separations larger than that corresponding to the maximum in the Kuiper or Duquennoy-Mayor distribution, which are presumably formed by processes different from those responsible for the closer binaries.

## 2. Construction of the catalog

A search of the literature was conducted, looking for high velocity, metal-poor wide binaries, since such samples are likely to be rich in halo stars. Most of the binaries in the new catalog stem from the lists of Ryan (1992), Allen et al. (2000), Chanamé & Gould (2004), and Zapatero-Osorio & Martin (2004). All listed data were checked, and updated when necessary. We selected the most reliable data for the distances, metallicities and radial velocities. All proper motions were checked in the Simbad database and non-common proper motion companions were eliminated (i.e., we omitted pairs with proper motions differing by more than the published values). The catalog includes 111 halo binaries from Allen et al (2000), 110 halo binaries from Chanamé & Gould (2004) 23 from Zapatero-Osorio & Martin (2004) and 7 from Ryan (1992), to give a total of 251 halo binary candidates.

In order to refine the sample, we constructed a reduced proper motion diagram (RPM), following Salim & Gould (2003) and ChG (2004). The RPM diagram for 251 candidate halo binaries is shown in Figure 1. The black diagonal line is the limit taken by ChG to separate disk from halo binaries. We note that this line excludes quite a few binaries for which galactic orbits from Allen et al. (2000) clearly imply their halo membership. Therefore, we draw a new limit, indicated by the dotted line, which includes most of the Allen et al. binaries with halo-like galactic orbits. Regardless of their position in the RPM diagram we exclude 40 binaries with galactic orbits such that they spend their whole lives within the disk, although their motions are clearly indicative of a thick disk or of an even dynamically hotter population. In this way, we end up with 212 binaries, most likely to belong to the galactic halo or thick disk.

To carry out the dynamical modelling of the evolution of halo binaries, the most useful quantity is the fraction of the lifetime that each binary spends far from the galactic disk. Thus, galactic orbits were calculated for all binaries with available radial velocities (at least for their primaries), a total of 150 systems. The Allen & Santillán (1991) galactic potential was used, and the orbits were calculated backwards in time for 13 Gyr. This allowed us to compute for each system  $t_d/t$ , the fraction of time spent within  $z = \pm 500$  pc.

The entire catalog is presented in Table 1. The entries are ordered by right ascension (J2000). Distances to the primaries were taken, when appropriate, from the Hipparcos catalog. Hipparcos distances were adopted for those stars with relative errors in their trigonometric parallaxes of less than 15%. For stars with larger errors, photometric distances were preferred, mostly taken from the lists of Nissen & Schuster (1991) and references therein, or by means of the polynomial used by ChG, adopting their photometry. For a few stars not found in those lists, spectroscopically derived distances were taken from either Ryan (1992) or Zapatero-Osorio & Martin (2004). Thus, most of the binaries listed in the catalog should have errors of less than 15% in their adopted distances.

Absolute visual magnitudes for the primaries were calculated from the adopted distances and the apparent visual magnitudes given in the respective catalogs. Absolute magnitudes for the secondaries were calculated as described in Allen et al. (2000) for their stars. They are mostly based on accurate photometry for the primary, and magnitude differences in two colors for the secondaries, a procedure which was shown by Allen et al. (2000) to yield reliable values for the absolute magnitudes of the secondaries. For binaries stemming from Chanamé & Gould their photometry was adopted. Secondaries from other sources are listed as in the original references.

Linear separations between the components were calculated from the angular separations and the adopted distances. The linear separations were transformed into expected values for the major semiaxes of the binaries by the statistical relation (Couteau 1960)

$$\langle a'' \rangle = 1.40s''.$$

Therefore, a binary with projected angular separation  $s''$  will have an expected major semiaxis  $\langle a \rangle$  given by

$$\langle a \rangle (\text{AU}) = \frac{1.40}{\pi} s''.$$

The above formula was derived by Couteau on theoretical grounds, assuming a random distribution of the geometrical elements of the orbit, as well as random times of passage through periastron. This relation turns out to be independent of the eccentricity distribution. Couteau also checked its observational validity based on more than 200 orbits, for which the constant turned out to be 1.411. A more recent empirical study (Bartkevičius 2008), based on data from the Catalog of Orbits of Visual Binary Stars (Hartkopf & Mason 2007) and the WDS (Mason et al. 2007). The result was  $\log \langle a \rangle - \log s$  ranging from 0.112 to 0.102. In view of the large uncertainties of the empirically derived values, and to facilitate comparisons with previous work, we shall use Couteau’s theoretical result.

In Table 1, we list in Column 1 the NLTT number of the primary, as well as the designation of its companion. In Column 2 we list alternative identifications of the primary. We provide, in order of preference, identifications in the Hipparcos, the HD, the Giclas (G) or the Wilson catalogs. Column 3 contains the identification of the secondary. Column 4 lists our best choice for the distance to the primary, as explained above. Columns 5 and 6 list the absolute magnitudes of the primary and secondary, respectively. Columns 7 and 8 the projected angular separation between the components and the expected value for the major semiaxis. The peculiar velocity of the binary is given in Column 9. This velocity is computed assuming a solar motion of (9, 12, 7) km s<sup>-1</sup>. The radial velocity used to compute the peculiar velocity in Column 9 is taken from various sources,

listed mostly in the Simbad database. The presence of undetected close companions to one or both members of the binary will affect the radial velocities, and thus the computed orbits. The observers have, in general, taken care to detect variations due to unseen companions. But the stars are faint and metal-poor, and thus observationally difficult. For the orbit computations we checked the published radial velocities to make sure we were using the systemic radial velocity -when available. Otherwise, we checked for radial velocity variations in the published data, and excluded a few systems with widely discrepant values. Columns 10 to 12 contain the main orbital parameters of the galactic orbit; we list the apocentric distance  $R_{\max}$ , the maximum distance from the galactic plane  $|z_{\max}|$  and the three-dimensional eccentricity  $e$  of the galactic orbit. In Column 13 we list  $t_d/t$ , the fraction of its lifetime the binary spends within the galactic disk ( $z = \pm 500$  pc). In the last column, the provenance of the binary is given (A = Allen et al. 2000; CG = Chaname & Gould, 2004; Z = Zapatero-Osorio et al., 2004; R = Ryan 1992).

### 3. Some statistical properties

#### 3.1. The distribution of absolute magnitudes

Figure 2 shows the frequency distribution of the absolute magnitudes of the primaries (full line) and the secondaries (dotted line) of our catalog. Note particularly the extension to the faint end of the magnitudes of the secondaries. This constitutes a sampling of the faint end of the main sequence for these metal-poor and presumably old stars. Observationally, these secondaries are challenging objects, being faint and having only a few lines in their spectra, but undoubtedly they are interesting and worthy of being included in observational programs.

#### 3.2. The distribution of peculiar velocities

Figure 3 is a histogram of the distribution of the peculiar velocities of the binaries. Note that most of the systems have peculiar velocities larger than  $60 \text{ km s}^{-1}$ , and thus can be considered to be good candidates to be bona fide thick disk or halo stars.

#### 3.3. The distribution of angular separations and expected major semiaxes

Figure 4 shows the cumulative distribution of the angular separations of the full sample of 251 low-metallicity high-velocity binaries. The straight line is a fit to the Oepik (1924) distribution  $f(s) = k/s$ . Figure 5 shows the same fit for the expected major semiaxes. In Allen et al.(2000,

2012), as well as here, we choose to display the distributions in cumulative form, since in this way we can apply directly the Kolmogorov-Smirnov (KS) test to quantitatively assess the probability that the observed distribution stems from a given theoretical distribution. Our choice of presentation of the angular distributions was criticized by ChG, who found a different exponent for the power law of their angular distributions. Since the matter remains controversial, we present below a brief discussion of the issue.

In Figure 6 we show the cumulative distribution of the ChG sample of 110 halo binaries. The straight line represents Oepik’s distribution, corresponding to a power-law exponent of  $-1$ . In Figure 7 we show the result of applying the Kolmogorov-Smirnov test to this sample. It is obvious that Oepik’s distribution shows an excellent fit to these stars up to an angular separation of 63 arc seconds, which includes 97 out of their 110 stars, leaving out those with the largest separations. We have performed the same test using an exponent of  $-1.6$ , as ChG do, and find a good fit, but only for binaries with separations larger than 3 arc seconds (94 binaries). Thus, it would appear that this controversy cannot be settled merely by goodness-of-fit arguments. We would interpret the departure from Oepik’s distribution as due to dynamical effects, an interpretation supported both from theoretical studies (Valtonen 1997 showed Oepik’s distribution to correspond to dynamical equilibrium) and from the observed distributions found for many independent samples of stars, and for groups of different ages (Poveda et al. 2006. Sesar et al. 2008; Lepine & Bongiorno 2007; Allen et al. 2000). We think the Oepik distribution is to be preferred for the following reasons.

1. It has been shown to hold for many different samples of wide binaries ( $a \geq 100$  AU) stemming from different and independent sources (Poveda et al. 2007, Sesar et al. 2008; Lepine & Bongiorno 2007; Allen et al. 2000). We show below that both the angular separations and the expected semiaxes of the candidate halo binaries in our improved catalog follow Oepik’s distribution. We also show that different subgroups of the catalog also follow Oepik’s distribution up to different limiting semiaxes.
2. It has been shown to hold up to different limiting separations for wide binaries of different ages (Poveda & Allen 2004; Poveda et al. 2006) which is exactly what one would expect from dynamical considerations.
3. It holds for a volume-complete sample of nearby wide binaries (Poveda & Allen 2004; Poveda et al. 2007) in the interval  $133 \text{ AU} < a < 2640 \text{ AU}$ .
4. It is thought to represent the primordial distribution of separations for wide binaries both from theoretical reasons (Valtonen 1997) and from observations (it holds for the youngest binaries up to their largest separations, see Poveda & Hernández-Alcántara 2003; Poveda et al. 2006).

5. We have shown above that it holds for the ChG halo binaries. Indeed, we found it holds also for their disk binaries, and explains in a natural way, as the result of dissolution effects, the flattening of their distribution, which ChG found puzzling, and for which they offered no explanation.

The cumulative frequency distribution of the angular separations for the more halo-like sample of 211 binaries is shown in Figure 8, that of the expected semiaxes in Figure 9. It is clearly seen that they follow Oepik’s distribution. We performed KS tests to support this assertion, and found that Oepik’s distribution holds up to angular separations of 160 arc seconds, and to expected semiaxes of 25 000 AU (0.12 pc). The latter test is shown in Figure 10.

To further refine our sample of halo candidates we integrated galactic orbits for all binaries with available radial velocities (150), and calculated the times they spend in the galactic disk, that is, between  $z$ -distances of  $\pm 500$  pc. Figures 11, 12 and 13 display the meridional orbits of three representative binaries. The cumulative frequency distribution of expected major semiaxes for this sample is shown in Figure 14, the result of the KS test in Figure 15. The preceding figures clearly show that Oepik’s distribution holds for all these subsamples, although it does so up to different values of the separations or major semiaxes.

Next, we separated the 150 binaries into three groups (each with an equal number of binaries), according to the time they spend within the galactic disk, as defined above. We refer to these groups as the most disk-like, the intermediate, and the most halo-like binaries. The average fraction of their lifetime the 50 most disk-like binaries spend in the disk is 100%, that of the most halo-like binaries is 18%. To maximize the contrast we disregarded the intermediate group.

Figures 16 and 17 show the cumulative frequency distribution of the expected major semiaxes for the most disk-like and the most halo-like groups. The corresponding KS tests are displayed in Figures 18 and 19. We see that the most disk-like binaries follow Oepik’s distribution up to an expected major semiaxis of 19,000 AU (0.09 pc), while the most halo-like binaries do so up to an expected semiaxis of 63,000 AU (0.31 pc).

These results confirm and reinforce the conclusions obtained in Poveda et al. (1997), Allen et al. (2000) and Poveda & Allen (2004), namely that (a) Oepik’s distribution is followed by many different samples of wide binaries; (b) that the maximum semiaxis up to which Oepik’s distribution holds is a function of the age of the group studied, as well as of the environment encountered by the binary along its galactic trajectory. Thus, for example, Poveda et al. (1994) were able to divide the binaries in their catalog in two groups, “probably young” ( $2 \times 10^9$  yr) and “probably old” ( $> 4.6 \times 10^9$  yr), according to a variety of age indicators. Poveda & Allen (2004) found Oepik’s law to be valid up to semiaxes of 8,000 AU for the young group, and up to only 2400 AU for the old group. For a very young ( $10^6$  yr) independent group of binaries in the Orion Nebula Cluster:

Poveda & Hernández-Alcantara (2003) found Oepik’s distribution to hold up to 45,000 AU.

The departure from Oepik’s distribution can be interpreted as due to the effects of dynamical perturbations, which tend to decrease the binding energy and thus increase the separation of the binary, until its ultimate dissolution. These effects, with the passage of time, will tend to eliminate the widest systems. Weinberg et al. (1987), Wasserman & Weinberg (1991) and more recently Jiang & Tremaine (2010) have modeled the evolution of disk binaries subject to perturbations by passing stars and molecular clouds. The former authors find galactic tides to have negligible effects for binaries with  $a < 0.65$  pc, the latter take tides into consideration for their widest binaries ( $a > 10^5$  AU). Our widest binaries would thus appear to be stable against galactic tides. The results of Weinberg et al. were found to be consistent with the distributions found for the youngest and oldest systems of the solar vicinity (Poveda et al. 1997). For the samples studied here, the departure from Oepik’s distribution sets in at much larger values than those obtained for even the oldest binaries of the solar vicinity. Similarly as was done in Allen et al. (2000) we interpret these larger values as due mainly to the relatively small time spent by our binaries within the galactic disk, where most of the perturbations occur. The most halo-like binaries in Allen et al. (2000) spent on average 26% of their lifetimes within the disk, and were found to follow Oepik’s distribution up to  $\langle a \rangle = 20,000$  AU (0.1 pc). The most halo-like binaries of our improved catalogue spend on average only 18% of their lifetime within the disk and follow Oepik’s distribution up to 63,000 AU (0.31 pc).

The question arises as to the effects of observational uncertainties on our results. Uncertainties in the distances will affect directly the inferred semiaxes, but not their distribution. The galactic orbits will be affected by uncertainties in the distances, proper motions and radial velocities. We have estimated the errors in the orbital parameters listed in Table 1 for a representative sample of binaries. To this end, we computed for each binary two extreme orbits by adding and subtracting all the uncertainties to the “central” values. This will provide an overestimate of the expected errors in the orbital parameters. The average resulting errors for this sample turned out to be 18% for  $R_{\max}$ , 14% for  $z_{\max}$  and 16% for  $e$ . Binary membership into the most halo-like and the most disk-like groups remained unchanged.

#### 4. Discussion and conclusions

By means of an extensive literature search we have compiled a list of 251 candidate halo wide binaries and present it in Table 1. Proper motions, radial velocities, photometric data and distances were carefully checked for each system. We found that the distribution of separations and major semiaxes for all the subgroups studied follows Oepik’s up to different limiting semiaxes. We computed galactic orbits for 150 binaries and obtained the fraction of their lifetimes spent within

the galactic disk. Separating the binaries into three groups, most disk-like, intermediate and most halo-like we find that the most disk-like binaries begin to depart from Oepik's distribution at an  $\langle a \rangle = 19,000$  AU, whereas the most halo-like do so at an  $\langle a \rangle = 63,000$  AU.

The great majority of the wide binaries in our catalog stem ultimately from Luyten's NLTT. The NLTT is quite complete up to visual magnitude 19, and for proper motions larger than 180 mas/yr. As such, it is a magnitude limited sample, and subject to the usual biases of such samples, namely, Malmquist, kinematical, and Lutz-Kelker biases. The rNLTT (Gould & Salim 2003; Salim & Gould 2003) covers the intersection of the First Palomar Observatory Sky Survey and the Second Incremental Release of the Two Micron Sky Survey, about 45% of the sky. As discussed by ChG, it is not necessary to have a volume-complete catalog, but a representative sample, with well understood selection effects. Our catalog, as well as previous ones, is far from complete. Certainly, many of the widest pairs will be missing. However, our main results on the distribution of semiaxes (showing the destructive effects of perturbers at large semiaxes), are not likely to be affected by incompleteness or biases. Oepik's distribution was previously found to hold for a volume-complete sample of nearby wide binaries (Poveda & Allen 2004, Poveda et al. 2007) in the interval  $133 \text{ AU} < \langle a \rangle < 1640 \text{ AU}$ . The same distribution was also found to hold (up to different values of the semiaxis) for different, independent samples of binaries, stemming from the LDS, the IDS and the catalog of nearby wide binaries of Poveda et al. (1994). Using a variety of age indicators, the latter binaries were separated into young and old groups; the limiting  $\langle a \rangle$  turned out to be 2400 AU for the oldest group and 7900 AU for the youngest group. Oepik's distribution was also found to hold up to  $\langle a \rangle = 30,000$  AU for a group of extremely young ( $10^6$  yr) wide binaries in the Orion Nebula Cluster (Poveda & Hernández-Alcántara 2003). It was also shown to hold for the disk and halo binaries of ChG (Poveda et al. 2007). We should mention that the Oepik distribution of separations was also found by Lepine & Bongiorno (2007) and Sesar (2008) in their catalogs. The consistency found between our present results and those previously found for many different and independent samples of binaries gives us confidence that incompleteness and selection effects are not significantly influencing our conclusions.

The origin of wide binaries has been a long-standing problem. Several mechanisms have been proposed for this problem, among which we can mention the dynamical unfolding of triple systems (Reipurth & Mikkola 2012), formation by capture of unbound stars in dissolving star clusters (Kouwenhoven et al. 2010, Moeckel & Clarke 2011, Perets & Kouwenhoven 2012), and the suggestion that they may be the sole remains of former moving groups or accreted structures in the galactic halo (Allen et al. 2007). Some of these scenarios have as a result a thermal distribution of eccentricities, and an Oepik-like distribution of semiaxes, and would thus accord better with the empirical findings on the distribution of separations of binaries found in different environments and having different ages. It is not clear which of these mechanisms -if any- would work for the halo binaries, but at this stage the scenarios involving cluster dissolution would seem more

plausible, since they result in a thermal distribution of eccentricities and-in some cases- an Oepik-like distribution fo semiaxes

Our present results are consistent with those found in Allen et al. (2000) with a smaller sample. In a companion paper we show that they allow us to obtain better estimates of the masses of the halo perturbers, and they should be also useful for other dynamical studies.

Acknowledgments. We thank A. Poveda, whose long-time interest in wide binaries inspired this work. MAM is grateful to UNAM-CEP for a graduate fellowship. Our thanks are also due to M. Hernández-Cruz for valuable assistance. This research used the Simbad database operated at CDS, Strasbourg, France.

## REFERENCES

- Alcock,C. Allsman,R.A. Alves,D. et al. 1998, ApJ, 499, L9
- Alcock, C., Allsman, R. A., Alves, D. R. et al. 2001, ApJ, 550, L169
- Allen,C. & Santillán, A. 1991, RMxAA 22, 255
- Allen, C., Poveda, A. & Herrera, M. A. 1997, in Visual Double Stars : Formation, Dynamics and Evolutionary Tracks. J.A. Docobo, A. Elipe, and H. McAlister. Dordrecht: Kluwer Academic, ASSL. 223, p. 133
- Allen, C., Poveda, A. & Herrera, M.A. 2000, A&A, 356, 529
- Allen, C. & Poveda, A. 2007, in Binary Stars as Critical Tools & Tests in Contemporary Astrophysics, IAU Symposium 240, Eds. W.I. Hartkopf, E.F. Guinan and P. Harmanec. Cambridge: Cambridge University Press, p. 405
- Monroy-Rodríguez, M. A. & Allen, C. 2013, ApJ, submitted
- Afonso, C., Albert, J. N., Andersen, J. et al. 2003, A&A, 400, 951
- Bartkevičius, A. 2008, Baltic Astronomy, 17, 209
- Chanamé, J. & Gould, A. 2004, ApJ, 601, 289
- Couteau, P. 1960, J. des Observateurs, 43, No. 3
- Duquennoy, A. & Mayor, M. 1991, A&A, 248, 485
- Gould, A. & Salim, S. 2003, ApJ, 582, 1001

- Hartkopf, W. I., & Mason B. D., 2007, Sixth Catalog of Orbits of Visual Binary Stars, WDS06, U.S. Naval Observatory, Washington
- Jiang, Y. & Tremaine, S. 2010, MNRAS, 401, 977
- Kouwenhoven, M. B., Goodwin, S. P., Parker, R. J. et al. 2010, MNRAS404, 1835
- Lacey, G. C., & Ostriker, J. P. 1985, ApJ, 299, 633
- Lépine, S. & Bongiorno, B. 2007, AJ, 133, 889
- Luyten, W. J. 1979, New Luyten Catalog of Stars with Proper Motions Larger than Two-Tenths of an Arcsecond (Minneapolis: Univ. Minnesota Press)
- Mason, B. D., Wycoff, G. L., Hartkopf, W.I. 2007, The Washington Double Star Catalog. WDS, U.S. Naval Observatory, Washington
- Moeckel, N., & Clarke, C. 2011, MNRAS, 415, 1179
- Nissen, P. E. & Schuster, W. J., 1991, A&A, 251, 457
- Oepik, E. J., 1924, Tartu Obs., 25,6
- Perets, H. & Kouwenhoven, M. B. 2012, ApJ, 750, 83
- Poveda, A. & Allen, C. 2004, IAU Colloquium 191 - The Environment and Evolution of Double and Multiple Stars, C. Allen & C. Scarfe, RMxAA 21, 49
- Poveda, A., Allen, C. & Hernández-Alcántara, A. 2007, in Binary Stars as Critical Tools & Tests in Contemporary Astrophysics, IAU Symposium 240, Eds. W.I. Hartkopf, E.F. Guinan and P. Harmanec. Cambridge: Cambridge University Press, p. 417
- Poveda, A., Allen, C. & Herrera, M. A. 1997, Visual Double Stars : Formation, Dynamics and Evolutionary Tracks. J.A. Docobo, A. Elipe, and H. McAlister. Dordrecht : Kluwer Academic, ASSL 223, 191
- Poveda, A. & Hernández-Alcántara, A. 2003, Stellar astrophysics. Sixth Pacific Rim Conference. Cheng, K. S., Leung, K. C. and Li. T. P. Dordrecht : Kluwer Academic, ASSL 298,111
- Poveda, A., Herrera, M.A., Allen, C., Cordero, G. & Lavalley, C. 1994, RMxAA 28, 43
- Quinn, D. P., Wilkinson, M. I., Irwin, M. J. et al. 2009, MNRAS, 396, 1, L11
- Raghavan, D., McAlister, H. A., Henry, T. et al. 2010, ApJS, 190, 1

- Reipurth, B. & Mikkola, S. 2012, *Nature*, 492, 221
- Ryan, S. G. 1992, *AJ*, 104, 1144
- Salim, S. & Gould, A. 2003, *ApJ*, 582, 1011
- Sesar, B., Ivezić, Z. & Jurić, M. 2008, *AJ*, 689, 1244
- Valtonen, M. 1997, *Visual Double Stars : Formation, Dynamics and Evolutionary Tracks*. J.A. Docobo, A. Elipe, and H. McAlister. Dordrecht : Kluwer Academic, ASSL. 223, 241
- Wasserman, I. & Weinberg, M. D. 1991, *ApJ*, 382, 149
- Weinberg, M. D., Shapiro S. L. & Wasserman I. 1987, *ApJ*, 312, 367
- Yoo, J., Chanamé, J. & Gould, A. 2004, *ApJ*, 601, 311
- Zapatero-Osorio, M.R. & Martín, E. L. 2004, *A&A*, 419, 167

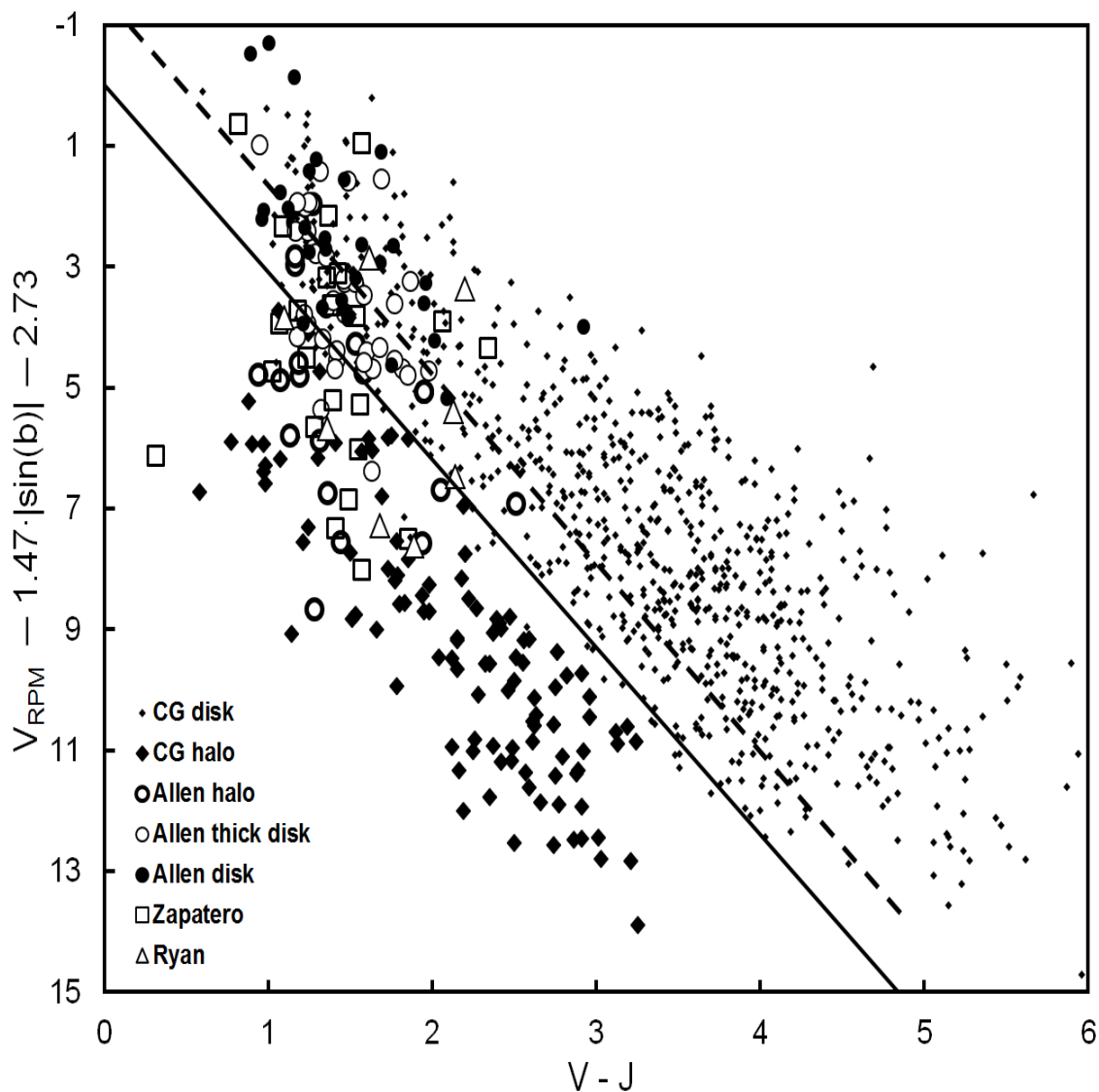


Fig. 1.— Reduced proper motion diagram for 251 halo wide binary candidates. The axes are defined as in ChG (their eq. 2). The  $V$ - $J$  plotted is that of the primaries. The vertical axis plots the reduced proper motion adjusted for galactic latitude  $b$ . Here  $V_{\text{RPM}} = V + 5 \log \mu$ , with  $V$  the  $V$ -magnitude and  $\mu$  the proper motion. The symbols denote the provenance from different catalogues. The full line was used by ChG to separate disk from halo binaries. However, this line excludes quite a number of binaries whose galactic orbits clearly indicate membership to the halo as was shown in Allen et al. (2000). To identify candidate halo binaries we shifted the ChG line so as to include these stars, as shown by the dashed line. Final halo membership was determined by computing the time the binaries spend within the galactic disk. See text for details

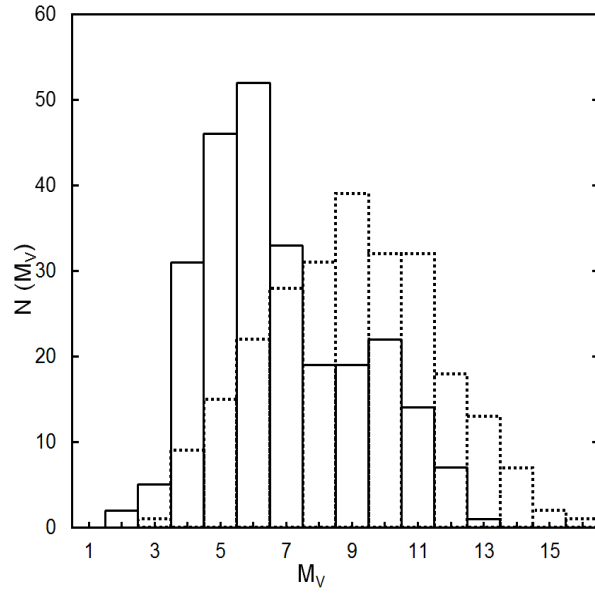


Fig. 2.— Frequency distribution of the absolute magnitudes of 251 halo wide binary candidates. The primaries (full line) and secondaries (dashed line) are shown. Note the extension of the magnitudes of the secondaries to the faint end of the diagram.

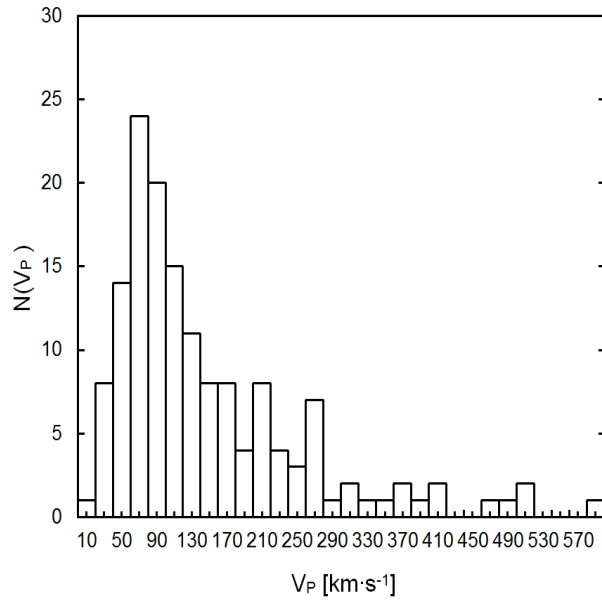


Fig. 3.— Frequency distribution of the peculiar velocities of 150 binaries with available radial velocities. Note that the majority of these stars have peculiar velocities much larger than  $65 \text{ km s}^{-1}$ , clearly indicating that halo binaries predominate in this sample.

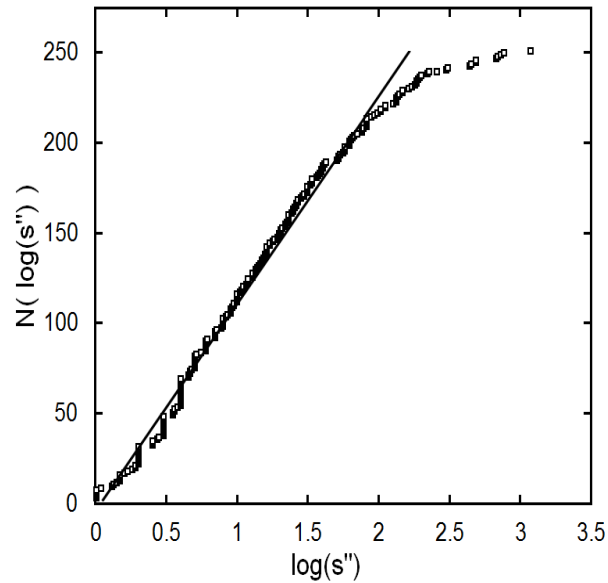


Fig. 4.— Cumulative distribution of the angular separations of 251 halo wide binary candidates. The full line is a fit to the Oepik distribution  $f(s) = k/s$ .

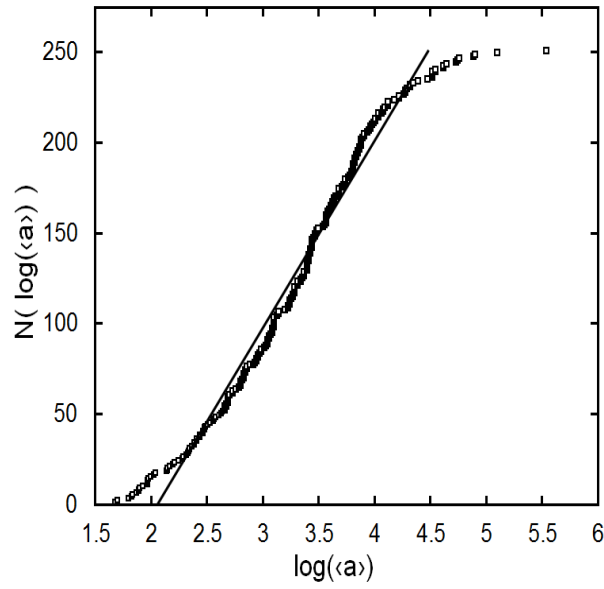


Fig. 5.— Cumulative distribution of the expected major semiaxes of 251 halo wide binary candidates. The full line is a fit to the Oepik distribution  $f(\langle a \rangle) = k\langle a \rangle^{-1}$ . Units for  $\langle a \rangle$  are AU.

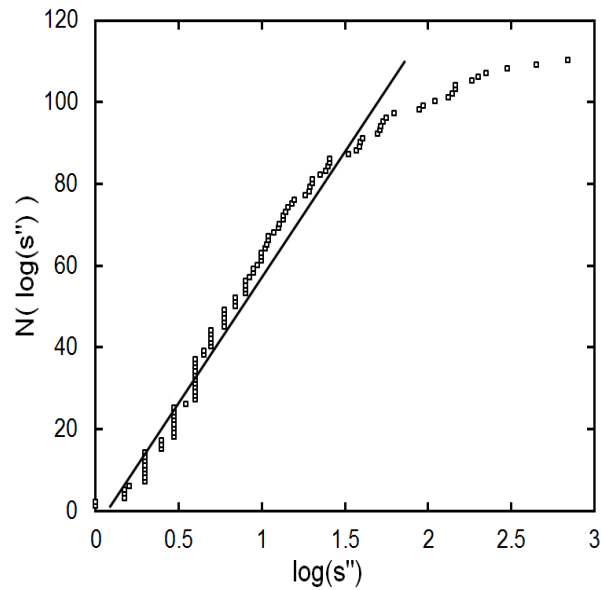


Fig. 6.— Cumulative distribution of the angular separations of the 110 ChG halo wide binaries. The full line is a fit to the Oepik distribution  $f(\langle a \rangle) = k\langle a \rangle^{-1}$ . The fit is seen to satisfactorily represent this sample.

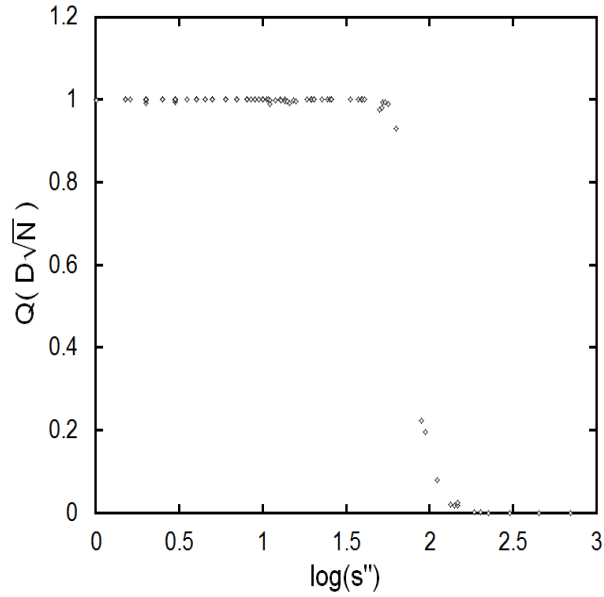


Fig. 7.— Result of applying the Kolmogorov-Smirnov test to the binaries of ChG shown in Figure 6. The coefficient of significance  $Q$  is plotted as the ordinate. The test shows that the fit is excellent up to a separation of 63 arc seconds (97 binaries), where it abruptly deviates from the Oepik distribution. See text for details.

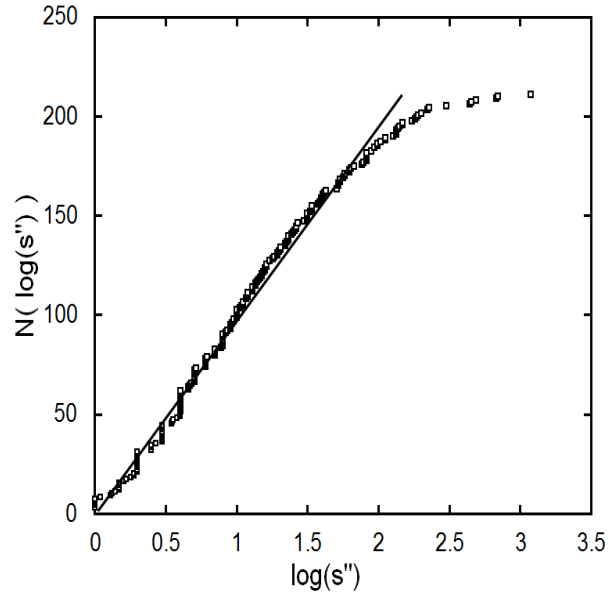


Fig. 8.— Cumulative distribution of the angular separations of the sample of 211 halo wide binary candidates. The full line is a fit to the Oepik distribution  $f(s) = k/s$ .

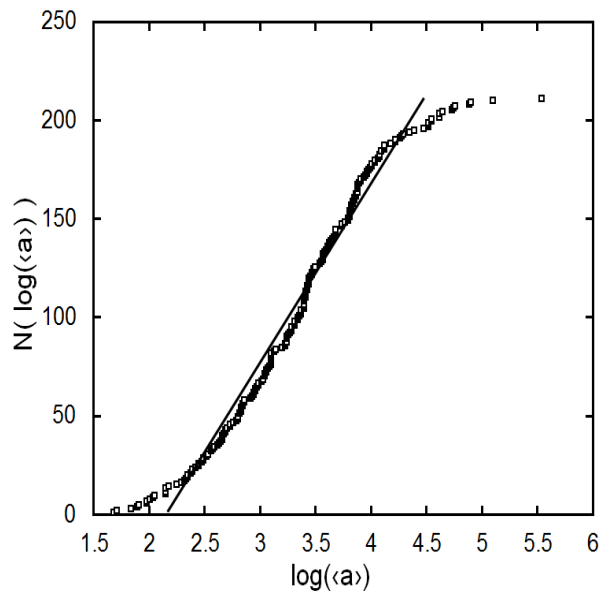


Fig. 9.— Cumulative distribution of the expected major semiaxes of the sample of 211 halo wide binary candidates. The full line is a fit to the Oepik distribution  $f(\langle a \rangle) = k\langle a \rangle^{-1}$ . Units for  $\langle a \rangle$  are AU.

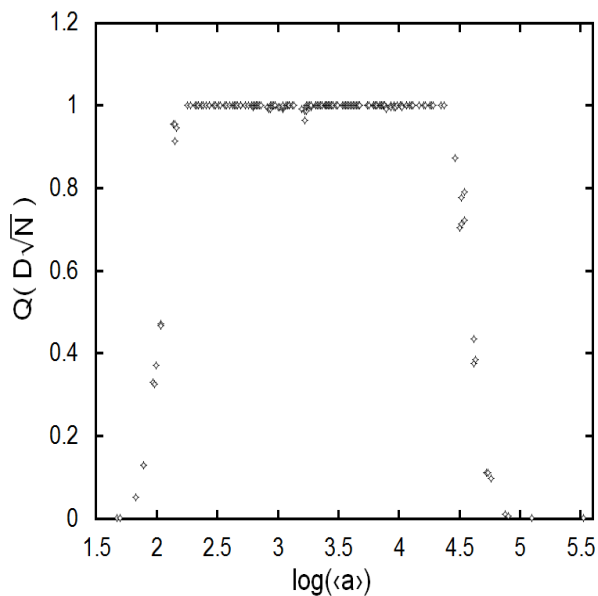


Fig. 10.— Result of the Kolmogorov-Smirnov test for the 211 binaries of Figure 9. Units for  $\langle a \rangle$  are AU. The test shows that the Oepik distribution holds up to an expected major semiaxis of 25 000 AU.

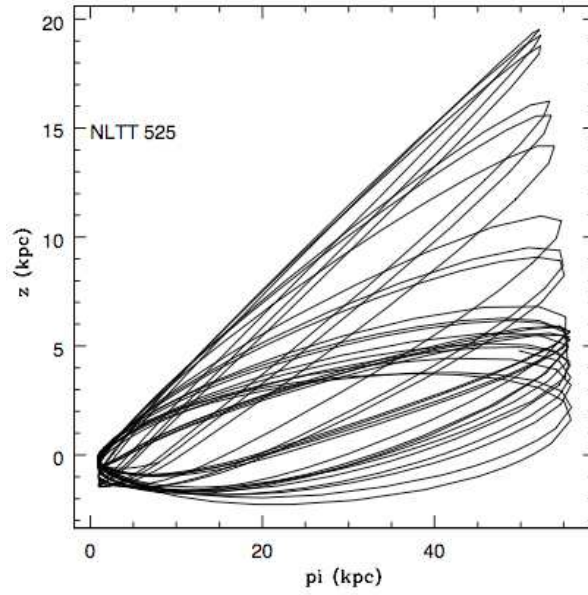


Fig. 11.— Meridional galactic orbit of the binary NLTT 525/526. This binary spends 15.7% of its lifetime within the galactic disk.

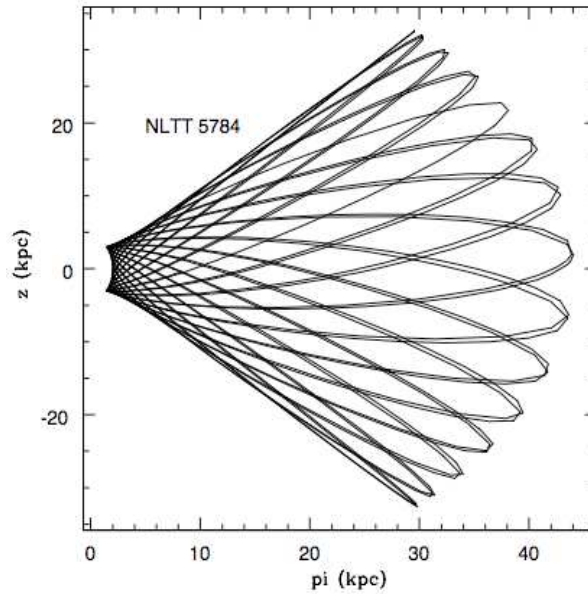


Fig. 12.— Meridional galactic orbit of the binary NLTT 5781/5784. This binary spends 1.9% of its lifetime within the galactic disk.

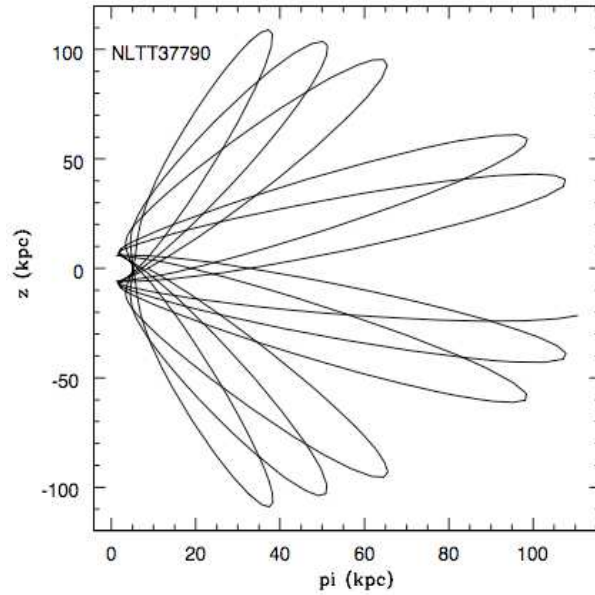


Fig. 13.— Meridional galactic orbit of the binary NLTT 37790/37787. This binary spends 0.3% of its lifetime within the galactic disk.

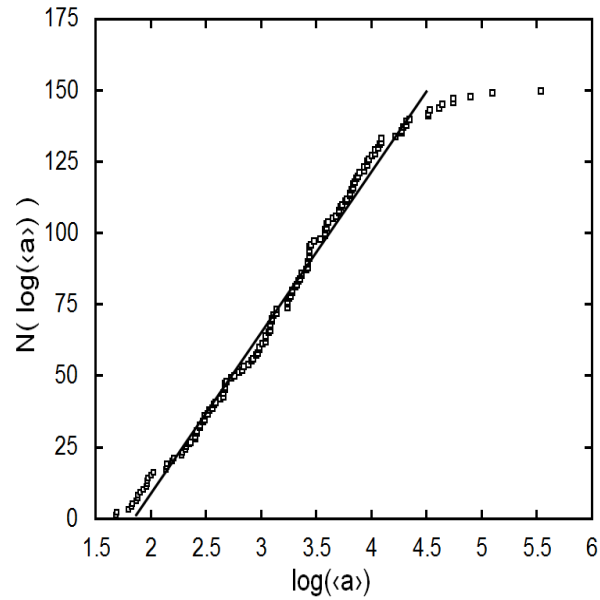


Fig. 14.— Cumulative distribution of the expected major semiaxes of 150 halo wide binary candidates with computed galactic orbits. Units for  $\langle a \rangle$  are AU. The full line is a fit to the Oepik distribution  $f(\langle a \rangle) = k/(\langle a \rangle)$

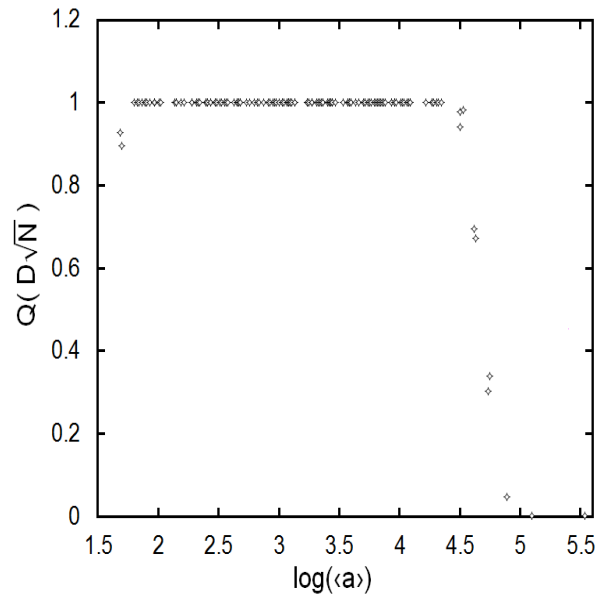


Fig. 15.— Result of applying the Kolmogorov-Smirnov test to the 150 binaries of Figure 14. The test shows that the fit is excellent up to an expected major semiaxis of 28,200 AU, and then abruptly deviates from the Oepik distribution. We interpret this departure as due to dynamical effects which tend to dissociate the widest binaries. See text for details.

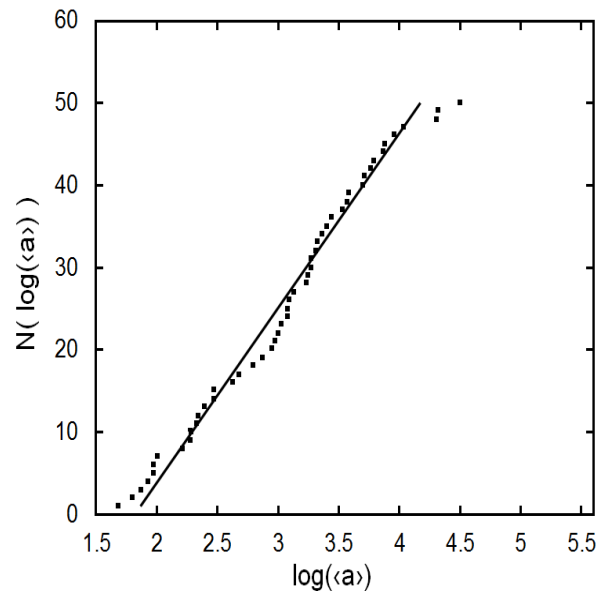


Fig. 16.— Cumulative distribution of the expected major semi-axes of 50 most disk-like wide binaries with computed galactic orbits. These binaries spend just about their entire lifetimes within the galactic disk. Units for  $\langle a \rangle$  are AU. The full line is a fit to the Oepik distribution  $f(\langle a \rangle) = k/\langle a \rangle$

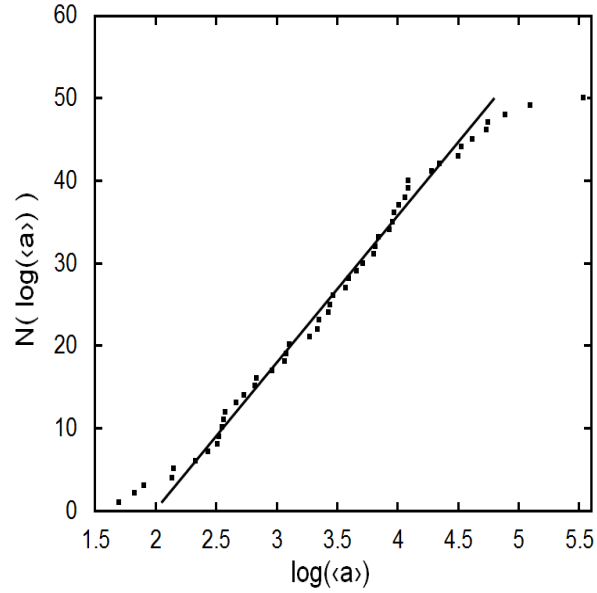


Fig. 17.— Cumulative distribution of the expected major semiaxes of 50 most halo-like wide binaries with computed galactic orbits. These binaries spend an average of 18% of their lifetimes within the galactic disk. Units for  $\langle a \rangle$  are AU. The full line is a fit to the Oepik distribution  $f(\langle a \rangle) = k/(\langle a \rangle)$ .

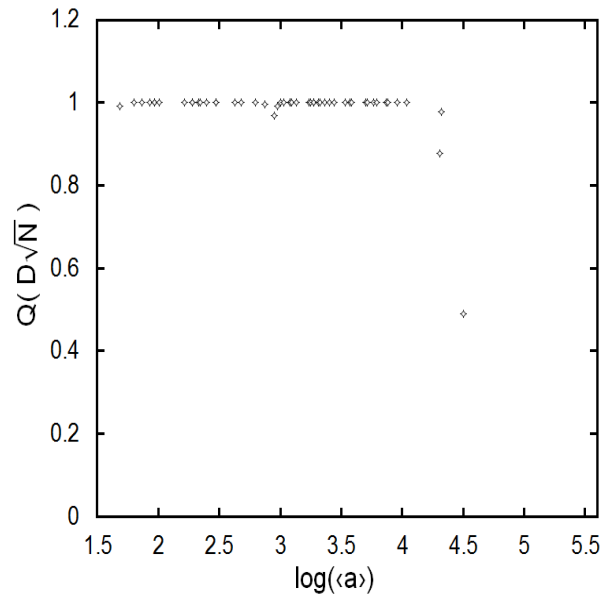


Fig. 18.— Result of applying the Kolmogorov-Smirnov test to the 50 most disk-like binaries of Figure 16. Units for  $\langle a \rangle$  are AU. The test shows that the fit is excellent up to an expected major semiaxis of 15 000 AU, and then abruptly deviates from the Oepik distribution.

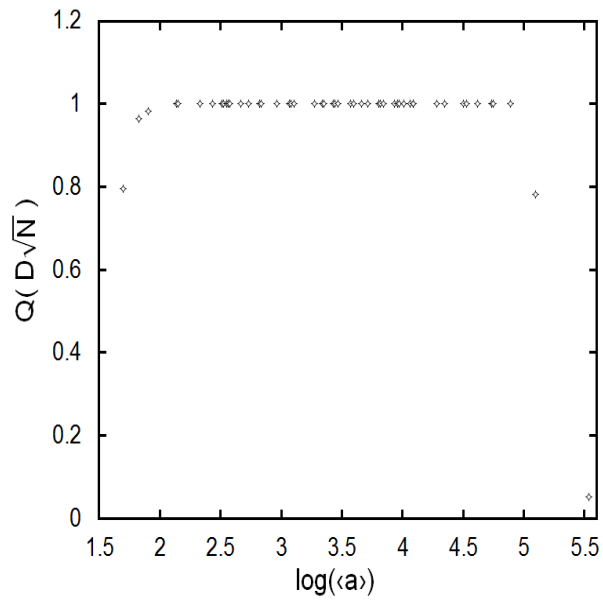


Fig. 19.— Result of applying the Kolmogorov-Smirnov test to the 50 most halo -like binaries of Figure 17. Units for  $\langle a \rangle$  are AU. The test shows that the fit is excellent up to an expected major semiaxis of 63 000 AU, and then abruptly deviates from the Oepik distribution. This result shows that Oepik’s distribution holds up to much larger values of the semiaxes as the binaries spend shorter fractions of their lifetimes within the galactic disk.

Table 1. Improved Catalog of Candidate Halo Wide Binaries

Primary	Other ID	Secondary	$d$	$M_V(p)$	$M_V(s)$	$s$	$\langle a \rangle$	$v_p$	$R_{max}$	$ z_{max} $	$e$	$t_d/t$	Cat
(1)	(2)	(3)	(pc)	(5)	(6)	(")	(AU)	(km/s)	(kpc)	(pc)	(12)	(13)	(14)
NLTT 58746		NLTT 58747	156	9.4	9.4	4	876						CG
NLTT 58812		NLTT 58813	435	6.2	6.2	2	1217						CG
NLTT 239		NLTT 240	496	10.0	10.0	10	6944						CG
NLTT 403	HIP 754	LP 348-62	45	4.5	8.8	30	1902	33.4	8.6	258	0.11	1.000	A
NLTT 525	HIP 911	NLTT 526	251	4.8	7.4	8.5	2986	361.3	31.6	3122	0.92	0.157	ACG
NLTT 1036		NLTT 1038	290	10.8	6.0	22.5	9135	213.0	9.8	7363	0.29	0.049	CG
NLTT 1412		NLTT 1416	104	9.5	6.7	51.5	7475						CG
NLTT 1645		NLTT 1647	219	7.5	9.9	20.2	6198						CG
NLTT 1806	HIP 2663	BD -35 170B	36	3.6	6.0	6	304	90.9	9.3	146	0.34	1.000	A
NLTT 1945	G 069-004	G 069-004 Ng	53	4.8	5.6	6.16	455	139.5	8.6	921	0.42	0.463	Z
NLTT 2056	G172-016	G172-016B	119	5.6	11.4	8.3	1383	123.7	9.5	523	0.70	0.969	Z
NLTT 2144		NLTT 2145	218	6.5	6.5	4	1220						CG
NLTT 2205		NLTT 2206	170	6.8	8.2	3	713						CG
NLTT 2324		NLTT 2325	198	8.5	8.5	2.5	694						CG
NLTT 2425		NLTT 2426	282	11.3	8.7	4	1580						CG
NLTT 2484	HIP 3550	LP 466-33	63	5.8	13.4	62	5467	69.8	9.7	350	0.22	1.000	A
NLTT 2963		NLTT 2964	397	10.7	11.3	2	1112						CG
NLTT 2989		NLTT 2990	107	9.9	9.9	1	149						CG
NLTT 3116	G 242-074 A	G 242-074 Bn	98	4.8	9.9	19.5	3182	124.5	8.6	1336	0.52	0.284	Z
NLTT 3252		NLTT 3253	503	9.5	10.7	10.8	7607						CG
	HIP 5140	LDS 34	82	4.4	7.8	23	2640	53.5	8.6	528	0.16	0.932	A
NLTT 3847		NLTT 3849	101	8.4	10.9	8	1127						CG
NLTT 4362	HIP 6130	BD -1 167B	28	5.8	9.7	28	1084	49.7	8.6	112	0.21	1.000	A
NLTT 4625		NLTT 4626	802	6.6	4.4	4	4492						CG
NLTT 4814	G 002-038	NLTT 4817	153	10.7	5.2	24.4	5139	303.0	12.9	8058	0.98	0.006	ACG
NLTT 5690	HIP 7869	LP 88-69	71	4.1	9.1	22	2198	183.7	8.6	4562	0.51	0.083	A
NLTT 5781		NLTT 5784	306	11.6	7.1	52.1	22320	380.4	44.2	32637	0.91	0.019	CG
NLTT 6529	HIP 9094	LP 709-81	34	3.8	9.3	29	1379	80.5	12.4	201	0.26	1.000	A
NLTT 7087	HIP 9971	BD 27 335B	57	6.2	6.8	22	1755	86.5	8.6	679	0.32	0.709	A
NLTT 7795	G4-16	LP 579-18	134	7.4	12.3	41	7689	147.8	8.6	468	0.67	1.000	A
NLTT 7845	HIP 11137	BD 14 387	57	5.1	5.6	34	2727	65.4	12.6	657	0.22	0.730	A
NLTT 8447	HIP 12114	BD 6 389B	7	6.5	12.4	170	1715	78.5	11.6	736	0.22	0.580	A
NLTT 8643	HIP 12411	LP 941-143	40	5.3	13.4	31	1738	81.1	8.9	311	0.32	1.000	A
NLTT 8720		NLTT 8721	205	7.2	7.2	6	1719						CG
NLTT 8753		NLTT 8759	206	9.8	10.9	146.3	42122						CG
NLTT 8997	HIP 13081	LP 354-414	22	5.8	13.8	20	626	17.7	8.6	68	0.07	1.000	A
NLTT 9360		NLTT 9361	216	10.3	10.1	18.3	5534						CG
NLTT 9798	HIP 14342	LP 470-9	100	3.6	7.6	1	140	104.5	8.7	2366	0.10	0.121	A
NLTT 9961		NLTT 9962	122	8.7	8.7	4	681						CG
NLTT 10356	HIP 15126	BD 0 549	79	5.7	11.3	78	8686	155.1	12.7	785	0.48	0.644	A
NLTT 10426	HIP 15253	BD 4 519	78	4.8	7.3	2	218	117.8	9.9	76	0.43	1.000	A
NLTT 10597	HIP 15371	BD -63 217	12	4.8	5.2	310	5241	74.0	9.5	321	0.24	1.000	A
NLTT 10514	HIP 15394	BD 14 550B	57	3.6	10.7	135	10772	72.4	8.8	673	0.23	0.669	A
NLTT 10536	HIP 15396	NLTT 10548	214	4.6	9.1	185.7	55410	417.5	9.6	5202	0.12	0.062	ACG

Table 1—Continued

Primary	Other ID	Secondary	$d$ (pc)	$M_V(p)$	$M_V(s)$	$s$ ( $''$ )	$\langle a \rangle$ (AU)	$v_p$ (km/s)	$R_{max}$ (kpc)	$ z_{max} $ (pc)	$e$	$t_d/t$	Cat
(1)	(2)	(3)	(4)	(5)	(6)	(7)	(8)	(9)	(10)	(11)	(12)	(13)	(14)
NLTT 10634	HIP 15572	BD 8 496	51	4.9	11.5	81	5752	60.5	8.7	444	0.21	1.000	A
NLTT 10701	HIP 15683	LP 412-34	73	6.6	13.2	26	2656	92.7	9.3	593	0.32	0.844	A
NLTT 10733	HD 20835	LP 155-70	79	4.3	10.5	10	1106	87.2	12.7	817	0.26	0.541	A
NLTT 10780		NLTT 10781	481	8.7	8.7	3	2020						CG
NLTT 10999		NLTT 11000	678	8.4	7.6	14	13288						CG
NLTT 11015		NLTT 11016	152	10.0	11.1	9	1920						CG
NLTT 11139		NLTT 11140	113	6.7	6.5	4	631						CG
NLTT 11124	HIP 16467	BD 43 744B	54	4.9	9.4	16	1205	70.2	8.9	318	0.27	1.000	A
NLTT 11330	L 91-93	L91-94	34	8.4	8.8	13	448						R
NLTT 11288		NLTT 11300	176	8.4	5.2	223.5	55082						CG
NLTT 11424	G6-22	LP 413-23	108	6.1	6.3	3	453	143.6	10.5	891	0.48	0.528	A
NLTT 11538		NLTT 11539	366	4.0	4.0	6	3072						CG
NLTT 11791	HIP 17666	NLTT 11792	25	6.9	6.3	8	274	151.4	9.6	1603	0.51	0.242	ACG
NLTT 12294		NLTT 12296	189	11.9	8.7	40.5	10691						CG
NLTT 12415	HIP 18824	LP 944-99	52	3.1	3.7	1.9	139	86.9	8.7	1094	0.25	0.341	A
NLTT 12415	HIP 18824		52	3.1	14.9	64	4678	86.9	8.7	1094	0.25	0.341	A
NLTT 12567	HIP 19255		21	5.6	3.8	720	20739	24.2	9.0	27	0.08	1.000	A
NLTT 12567	HIP 19255	BD 37 878B	21	5.6	7.4	3.6	74	24.2	9.0	27	0.08	1.000	A
NLTT 12863	HIP 19849	BD -7 781A	5	5.9	10.8	82	578	111.2	12.7	624	0.34	0.815	A
	Lp 230-119	Lp 230-125	84	8.5	8.5	31	2606						R
NLTT 13455	HD 283702	BD 26 727B	80	6.4	8.5	16	1791	92.1	8.6	144	0.41	1.000	A
NLTT 13968		NLTT 13970	148	5.7	12.9	20.3	4209						CG
NLTT 14005	G85-17	NLTT 13996	103	5.7	12.6	133	19173	101.9	8.7	2000	0.20	0.157	A
NLTT 14142	HD 31208	BD 7 754B	34	5.5	5.8	16	761	53.0	8.7	41	0.22	1.000	A
NLTT 14407		NLTT 14408	47	8.5	11.2	11	725						CG
NLTT 14658		NLTT 14659	174	5.8	5.8	2.5	609						CG
NLTT 14867	HIP 24819	BD -3 1061B	17	6.6	6.6	4	94	90.6	9.7	363	0.31	1.000	A
NLTT 14943	HIP 25137	LP 638-4	62	5.3	9.1	76	6591	80.6	12.4	1196	0.22	0.307	A
NLTT 15008		NLTT 15009	144	10.4	12.9	12.7	2554						CG
NLTT 15113	G 99-8	G99-9	114	8.0	9.5	83	9467						R
NLTT 15262	HIP 26018	BD 19 953	46	5.5	7.3	4	258	56.5	8.7	607	0.16	0.766	A
NLTT 15426	HIP 26501	BD -46 1936B	25	5.3	7.9	5.5	194	63.1	10.4	253	0.19	1.000	A
NLTT 15512	HIP 26907	BD 2 1041B	31	6.1	11.2	53	2325	88.9	8.5	130	0.40	1.000	A
NLTT 15501		NLTT 15509	210	10.6	11.0	141	41454	328.6	28.2	1481	0.85	0.374	CG
NLTT 15664		NLTT 15665	45	11.8	11.8	3.5	222						CG
NLTT 15953		NLTT 15954	122	10.4	13.3	14.4	2466						CG
NLTT 15973	HIP 28671	LTT 9457	39	6.4	9.8	7	382	258.6	16.4	1822	0.76	0.220	A
NLTT 16062	HIP 28940	BD 34 567	70	6.6	10.4	12	1176	265.5	11.8	6401	0.94	0.103	A
NLTT 16184		NLTT 16185	457	5.9	7.4	4.5	2879						CG
NLTT 16394		NLTT 16407	348	4.5	7.6	698.5	340309	481.5	144.0	88786	0.90	0.003	CG
NLTT 16629		NLTT 16631	55	6.4	10.5	434.1	33416	179.6	8.9	2562	0.29	0.125	CG
NLTT 16747	HIP 31740	LP 160-41	84	5.5	13.7	62	7280	131.8	9.9	784	0.46	0.619	A
NLTT 16948	HIP 32423	R 419	25	6.8	11.0	31	1084	70.7	13.7	916	0.24	0.458	A
NLTT 17017	HIP 32650	LDS 5686	50	4.4	12.4	27	1893	128.3	12.6	1116	0.37	0.376	A

Table 1—Continued

Primary	Other ID	Secondary	$d$	$M_V(p)$	$M_V(s)$	$s$	$\langle a \rangle$	$v_p$	$R_{max}$	$ z_{max} $	$e$	$t_d/t$	Cat
(1)	(2)	(3)	(pc)	(5)	(6)	(")	(AU)	(km/s)	(kpc)	(pc)	(12)	(13)	(14)
NLTT 17116	G 192-57	LP122-11	238	5.4	8.3	103	24538						R
NLTT 17382	HIP 34065	BD -43 2907	16	4.5	5.6	21	478	75.7	8.8	156	0.30	1.000	A
NLTT 17382	HIP 34065	BD -43 2904	16	4.5	8.1	193	4389	75.7	8.8	156	0.30	1.000	A
NLTT 17675	HIP 35599	LP 58-160	85	4.3	11.9	58	6868	117.9	10.0	175	0.42	1.000	A
NLTT 17770	HIP 35756	LP 359-227	180	4.1	10.4	34	8565	262.7	11.7	8661	0.96	0.158	A
NLTT 17890	HIP 36165	BD -34 3610	40	4.0	4.6	17	944	76.5	9.4	686	0.22	0.635	A
NLTT 17907	HIP 36357		18	2.9	10.6	2.8	69	39.6	10.9	259	0.14	1.000	A
NLTT 17907	HIP 36357	BD+32 1562	18	6.5	2.9	757	18594	39.6	10.9	259	0.14	1.000	A
NLTT 18247		NLTT 18248	110	6.6	6.2	2	307						CG
NLTT 18346	HIP 37671	NLTT 18347	167	5.1	4.3	11.9	2805	290.3	21.6	17469	0.52	0.028	ACG
NLTT 18775	G 90-036	G090-036B	293	5.4	8.8	1.67	685	515.8	429.1	53116	0.96	0.020	Z
NLTT 18798		NLTT 18799	154	8.9	4.9	12.9	2788						CG
NLTT 19053		NLTT 19054	460	4.3	4.3	4	2578						CG
NLTT 18924		NLTT 18931	79	10.3	5.5	110.4	12210	155.0	9.0	1958	0.44	0.185	CG
NLTT 19210	G 40-14	BD 30 4982B	235	4.5	10.8	98	32233	413.2	16.4	1444	0.70	0.327	A
NLTT 19979		NLTT 19980	344	7.9	10.2	19.6	9439	228.1	15.0	8120	0.92	0.135	CG
NLTT 20201		NLTT 20202	248	11.4	8.1	33.4	11581						CG
NLTT 20699		NLTT 20700	136	9.7	6.8	5	950						CG
NLTT 20892		NLTT 20894	270	9.2	8.0	8	3023						CG
NLTT 20979	G 09-047	G009-047B	89	2.9	11.6	81.93	10217	162.8	10.1	1617	0.62	0.233	Z
NLTT 21061	G116-009	G116-009B	265	7.2	11.2	10.08	3744	105.7	9.6	5395	0.89	0.237	Z
NLTT 21351		NLTT 21352	699	3.6	3.6	2.5	2445						CG
NLTT 21914		NLTT 21915	420	10.1	9.2	8	4703						CG
NLTT 21999	HIP 46853		14	2.5	12.9	5	94	56.2	9.3	220	0.18	1.000	A
NLTT 22230	HIP 47225		34	4.3	9.4	4	191	49.9	8.6	437	0.16	1.000	A
NLTT 22301		NLTT 22302	378	9.3	7.8	13.6	7187						CG
NLTT 22525		NLTT 22526	416	6.2	4.5	5	2908						CG
NLTT 22726	G 43-7	LP 548-41	120	6.3	13.0	15	2519	178.4	13.9	340	0.56	1.000	A
NLTT 23500	HIP 49668	AB	38	4.4	8.1	4.7	248	55.5	8.7	620	0.15	0.705	A
NLTT 23895	BD+23 2207A	BD+23 2207Bv	23	4.0	9.6	7.72	245	206.9	9.3	150	0.16	1.000	Z
NLTT 23937		NLTT 23938	289	9.7	9.7	1	405						CG
NLTT 24638		NLTT 24639	441	5.9	9.9	6	3700						CG
NLTT 25233		NLTT 25234	183	9.8	6.3	9	2300						CG
NLTT 25403		NLTT 25404	177	6.8	5.2	25.9	6415						CG
NLTT 25582	HIP 53165		55	4.4	6.1	1	77	73.3	9.7	403	0.23	1.000	A
NLTT 25623		NLTT 25624	247	8.4	8.4	3	1038						CG
NLTT 26709		NLTT 26710	85	12.0	12.0	1.5	178						CG
NLTT 27069	G 45-48	BD 6 2436B	92	5.4	8.9	18	2318	103.7	14.5	602	0.33	0.853	A
NLTT 27182		NLTT 27188	128	9.4	7.8	39.1	7030						CG
NLTT 28236	G176-046	G176-046D	127	7.1	12.0	4.8	853	100.3	8.7	989	0.63	0.517	Z
NLTT 28289		NLTT 28290	120	10.3	11.1	10	1686						CG
NLTT 28512	HIP 57443	VB 5	9	5.1	15.7	23	297	58.4	9.4	139	0.20	1.000	A
NLTT 29142	HIP 58401	LP 158-35	32	6.4	13.4	23	1027	189.1	8.5	24	0.88	1.000	A
NLTT 29424		NLTT 29425	481	9.3	9.3	3	2020						CG

Table 1—Continued

Primary	Other ID	Secondary	$d$	$M_V(p)$	$M_V(s)$	$s$	$\langle a \rangle$	$v_p$	$R_{max}$	$ z_{max} $	$e$	$t_d/t$	Cat
(1)	(2)	(3)	(pc)	(5)	(6)	( $''$ )	(AU)	(km/s)	(kpc)	(pc)	(12)	(13)	(14)
NLTT 29556	HIP 58962	BD 19 1185B	135	4.7	7.8	1.8	340	266.9	9.5	5962	0.93	0.232	A
NLTT 29553	HIP 58962	NLTT 29556	135	7.8	4.5	11	2267	266.9	9.5	5962	0.93	0.232	ACG
NLTT 29665	HIP 59126	LP 494-38	42	6.5	15.0	66	3836	71.5	8.9	206	0.28	1.000	A
NLTT 29742	HIP 59233	LP 376-84	56	5.8	10.3	16	1254	91.6	10.5	329	0.29	1.000	A
NLTT 29798		NLTT 29799	240	7.7	7.7	2	672						CG
NLTT 29860		NLTT 29862	371	5.0	5.0	7	3635						CG
NLTT 29957	HIP 59532	LPM 416AB	34	4.8	10.3	2	95	113.3	13.2	743	0.34	0.662	A
NLTT 30746		NLTT 30750	169	10.4	10.8	19.4	4593						CG
NLTT 30792		NLTT 30795	370	10.5	7.8	146.7	75889						CG
NLTT 30837		NLTT 30838	340	11.4	4.9	15.7	7473						CG
NLTT 31465	G 59-032	G059-032B	48	5.5		112.03	7535	211.1	10.6	325	0.32	1.000	Z
NLTT 31648	HIP 62041	LP 377-97	75	6.5	13.7	12	1260	68.6	8.6	375	0.28	1.000	A
NLTT 31891		NLTT 31892	227	7.4	7.4	4	1271						CG
NLTT 31917		NLTT 31918	208	8.9	8.9	3	873						CG
NLTT 32187	HIP 62882	VBS 2	80	3.8	7.8	1.9	213	356.1	22.0	9995	0.94	0.055	A
NLTT 32423	HIP 63239	LP 436-66	73	5.5	4.7	58	5934	84.5	11.6	320	0.26	1.000	A
NLTT 33175	HIP 64345	LDS 3735	61	4.8	9.1	82	7015	164.4	14.6	1898	0.47	0.217	A
NLTT 33209	HIP 64386	LDS 947	70	5.6	7.1	446	43652	117.5	11.0	511	0.37	0.980	A
NLTT 33282		NLTT 33283	188	8.7	9.2	10	2635						CG
NLTT 33527	HIP 64797	BD 17 2611B	11	6.3	10.1	4	63	48.8	11.1	50	0.17	1.000	A
NLTT 34609	G255-038 A	G 255-038 Bq	45	6.6	10.3	14.34	901	183.1	9.3	327	0.29	1.000	Z
NLTT 35210	HIP 67246	LDS 3101	31	3.9	7.5	486	20828	68.0	9.1	195	0.25	1.000	A
NLTT 35299	HIP 67408	BD -35 9019B	28	4.3	8.2	12	475	59.8	8.8	33	0.24	1.000	A
NLTT 35953		NLTT 35954	452	10.6	9.8	10.5	6641						CG
NLTT 35991		NLTT 36000	52	11.7	9.1	133.4	9792						CG
NLTT 36418	HIP 69220	BD -44 9130	49	4.9	11.0	4	273	79.8	9.0	795	0.24	0.511	A
NLTT 36418	HIP 69220	BD 44 9130	49	4.9	7.0	57	3893	79.8	9.0	795	0.24	0.511	A
NLTT 36674		NLTT 36675	174	9.4	9.4	2	487						CG
NLTT 37675		NLTT 37676	162	9.3	9.3	2	454						CG
NLTT 37787		NLTT 37790	193	9.9	6.4	200.9	54283	470.0	115.2	109015	0.92	0.003	CG
NLTT 37935	HIP 71505	LP 500-101	99	4.6	5.7	27	3741	140.5	11.3	158	0.46	1.000	A
NLTT 37997	HIP 71735	LDS 485	27	5.2	9.0	490	18825	74.1	11.1	922	0.19	0.422	A
NLTT 38115		NLTT 38116	427	3.9	3.9	6	3583						CG
NLTT 38195	G 66-022	BD +06 2932 B	73	6.1	9.0	3.6	443	267.6	18.1	10301	0.96	0.137	Z
NLTT 39117		NLTT 39119	375	11.1	5.7	56.7	29736						CG
NLTT 39442	HIP 74199	LP 424-27	132	6.4	6.6	677	125073	306.7	15.6	7088	0.87	0.075	A
NLTT 39456	HIP 74235	NLTT 39457	29	6.7	7.1	300.7	12380	592.2	67.0	6410	0.86	0.088	ACG
NLTT 39616	HIP 74549	BD -40 9410	51	4.9	5.0	17	1213	81.6	9.4	216	0.28	1.000	A
NLTT 39941	HIP 75069	Ross 1050	45	6.0	9.3	190	11856	58.9	9.5	656	0.14	0.638	A
NLTT 40737		NLTT 40738	540	8.9	8.9	1.6	1209						CG
NLTT 40901		NLTT 40902	90	10.0	12.0	4	501						CG
NLTT 41756	G 16-25	VB 6	256	6.3	8.7	1.5	537	515.9	19.9	6958	0.43	0.060	A
NLTT 42554		NLTT 42555	262	7.7	10.2	5	1832						CG
NLTT 42846	HIP 80630		66	5.5	11.0	23	2125	186.8	10.8	313	0.67	1.000	A

Table 1—Continued

Primary	Other ID	Secondary	$d$	$M_V(p)$	$M_V(s)$	$s$	$\langle a \rangle$	$v_p$	$R_{max}$	$ z_{max} $	$e$	$t_d/t$	Cat
(1)	(2)	(3)	(pc)	(5)	(6)	( $''$ )	(AU)	(km/s)	(kpc)	(pc)	(12)	(13)	(14)
NLTT 42969	LP745-22	LP745-23	31	9.1	9.6	126	3905						R
NLTT 43097	G153-067	G 017-027j	48	6.2	10.5	1170.7	79139	162.7	9.4	5692	0.69	0.074	Z
NLTT 43594		NLTT 43595	158	6.6	8.0	6	1331						CG
NLTT 44127	HIP 83591	BD -4 4226	11	7.5	9.4	184	2770	74.8	8.9	300	0.28	1.000	A
NLTT 44256		NLTT 44257	139	11.2	11.2	1.5	292						CG
NLTT 44816	HIP 85378	NLTT 44814	69	4.3	5.5	67	6463	128.9	9.0	1489	0.43	0.253	A
NLTT 45000		NLTT 45001	332	11.4	11.1	9.5	4408						CG
NLTT 45605	HIP 87533		66	3.5	7.0	1	93	133.3	9.2	526	0.51	0.955	A
NLTT 45995	HIP 88937		40	4.6	10.1	4.6	260	56.5	8.5	210	0.23	1.000	A
NLTT 46029	HIP 89000		47	2.3	8.3	7.2	473	36.2	8.5	223	0.13	1.000	A
NLTT 46029	HIP 89000		47	2.3	6.6	104	6808	36.2	8.5	223	0.13	1.000	A
NLTT 46118	G204-049	G204-049B	86	6.2	10.5	2.7	324	218.3	12.0	1163	0.50	0.377	Z
NLTT 46748	HIP 91360	LP 690-95	37	5.5	11.9	36	1868	76.1	8.5	57	0.35	1.000	A
NLTT 46857	HIP 91605		24	6.8	10.3	9	301	108.2	13.2	484	0.33	1.000	A
NLTT 47194	HIP 92960	LP 691-17	75	5.8	10.6	33	3452	145.6	11.3	311	0.47	1.000	A
NLTT 47748		NLTT 47749	254	9.1	8.5	7	2490						CG
NLTT 47955	HIP 96333	LP 869-10	72	4.7	9.3	40	4031	102.5	8.8	157	0.43	1.000	A
NLTT 47955	HIP 96333		72	4.7	6.7	1.4	141	102.5	8.8	157	0.43	1.000	A
NLTT 47984	HIP 96402		39	4.6	10.8	3	164	64.3	8.7	257	0.25	1.000	A
NLTT 48072		NLTT 48073	44	11.7	11.7	4.5	276						CG
NLTT 48140		NLTT 48142	171	4.1	6.6	25.7	6135						CG
NLTT 48402	HIP 97940	BD 1 4135	47	5.4	5.7	163	10802	57.2	9.1	290	0.19	1.000	A
NLTT 48402	HIP 97940		47	5.4	8.1	76.8	5089	57.2	9.1	290	0.19	1.000	A
NLTT 48652	HIP 98767	BD 29 3872B	16	4.7	13.8	178	3959	64.4	8.5	990	0.11	0.346	A
NLTT 48686	HIP 99029		75	4.9	6.6	2	210	98.4	8.9	316	0.39	1.000	A
NLTT 48832	HIP 99461	LPM 452	6	6.4	12.5	8	68	130.1	11.3	1139	0.38	0.351	A
NLTT 49312	HIP 100970		37	4.0	7.5	3	157	96.0	9.2	425	0.35	1.000	A
NLTT 49486		NLTT 49487	115	9.8	7.0	4	645						CG
NLTT 49474		NLTT 49477	146	5.3	12.4	89.1	18268						CG
NLTT 49562	G 262-021	G 262-022r	281	6.7	7.2	29.54	12155	370.5	40.0	27828	0.98	0.031	ZR
NLTT 49624		NLTT 49625	254	7.8	7.8	1.5	533						CG
NLTT 49746	G 230-047A	G 230-047B1	78	5.7	10.7	11.63	1159	226.6	10.9	1007	0.27	0.401	Z
NLTT 49819		NLTT 49821	289	7.1	5.9	25.1	10165						CG
NLTT 49903	G 230-049A	G 230-049Bm	57	4.7	4.8	1.33	106	234.9	11.7	276	0.30	1.000	Z
NLTT 50559	HIP 104214	BD 38 4344	4	7.5	8.3	24.6	86	95.0	10.1	13	0.32	1.000	A
NLTT 50761	HIP 104660		56	4.3	6.3	1.3	101	142.3	10.9	476	0.48	1.000	A
NLTT 50824		NLTT 50827	375	7.0	4.9	62.7	32910						CG
NLTT 51353	HIP 106074	Wolf 478	51	7.6	9.1	1.1	80	278.0	8.8	1919	0.80	0.234	A
NLTT 51353	HIP 106074	LDS 518	51	7.6	12.1	0.7	50	278.0	8.8	1919	0.80	0.234	A
NLTT 51459	G26-8	LP 637-61	72	6.4	9.9	9.5	957	104.9	9.9	52	0.37	1.000	A
NLTT 51479	HIP 106335	LP 564-23	49	6.9	8.6	0.7	48	133.1	10.9	97	0.45	1.000	A
NLTT 51479	HIP 106335	BD 31 3025	49	6.9	12.5	132	9119	133.1	10.9	97	0.45	1.000	A
NLTT 51780	G 93-027	G093-027B	136	6.0	8.7	3.52	672	259.8	14.4	2596	0.45	0.149	Z
NLTT 51964	G188-022	G188-022B	130	4.5	11.4	5.08	922	218.1	12.7	1710	0.62	0.240	Z

Table 1—Continued

Primary	Other ID	Secondary	$d$ (pc)	$M_V(p)$	$M_V(s)$	$s$ ( $''$ )	$\langle a \rangle$ (AU)	$v_p$ (km/s)	$R_{max}$ (kpc)	$ z_{max} $ (pc)	$e$	$t_d/t$	Cat
(1)	(2)	(3)	(4)	(5)	(6)	(7)	(8)	(9)	(10)	(11)	(12)	(13)	(14)
NLTT 51992		NLTT 51993	1138	8.0	7.6	3	4779						CG
NLTT 52131	G214-001	G214-001B	170	5.9	11.7	5.14	1221	167.1	10.3	1640	0.64	0.237	Z
NLTT 52532		NLTT 52538	249	7.9	11.9	37.3	12994						CG
NLTT 52648		NLTT 52649	954	6.0	6.0	5	6679						CG
NLTT 52786		NLTT 52787	167	5.8	5.3	2	468	162.4	9.7	3623	0.58	0.123	CG
NLTT 52864	G 18-24		119	6.6	11.0	99	16489	201.9	10.4	757	0.76	0.724	A
NLTT 53061		NLTT 53062	39	9.6	9.6	2	110						CG
NLTT 53254		NLTT 53255	106	9.2	9.6	53.8	7980						CG
NLTT 53376		NLTT 53377	270	9.6	11.8	5	1886						CG
NLTT 53617		NLTT 53618	118	10.1	10.1	3	494						CG
NLTT 54517	LP520-70	LP520-71	107	5.5	8.1	229	24591						R
NLTT 54708	LP521-3	LP521-4	151	5.2	7.1	38	5741						R
NLTT 55277		NLTT 55278	396	5.9	8.6	4	2218						CG
NLTT 55287	HIP 113231	BD -8 5980B	35	5.3	13.6	42	2047	81.0	9.8	154	0.28	1.000	A
NLTT 55326	HIP 113280	BD 16 4838B	32	6.7	8.3	5	225	28.4	8.5	250	0.09	1.000	A
NLTT 55719		NLTT 55720	104	12.7	12.7	3	435						CG
NLTT 55912	G 028-040	LP 581-80	124	5.8	8.9	15.81	2467	178.9	10.5	230	0.53	1.000	Z
NLTT 55994		NLTT 55997	234	5.4	10.4	50	16392						CG
NLTT 56357	HIP 114962	BD -36 13940B	39	6.2	13.8	15	819	237.9	12.9	575	0.78	0.964	A
NLTT 56335	HIP 114980	BD -67 2593	27	6.8	6.6	71	2709	82.5	8.5	380	0.35	1.000	A
NLTT 56392	HIP 115012		55	4.2	5.8	1	77	72.4	8.9	155	0.29	1.000	A
NLTT 56856	HIP 115684	LP 346-72	89	4.9	7.2	260	32230	103.4	10.7	334	0.32	1.000	AZ
NLTT 56926	G216-045	G216-045B	143	5.5	14.0	31.45	6305	257.1	14.4	94	0.43	1.000	Z
NLTT 57220	G128-077	G128-077B	209	6.8	9.6	9.18	2692	210.8	12.3	1047	0.59	0.472	Z
NLTT 57259		NLTT 57262	222	12.4	9.6	13.5	4193						CG
NLTT 57309	HIP 116421		32	4.3	11.4	8	362	131.2	9.0	1407	0.46	0.269	A
NLTT 57558		NLTT 57559	223	10.7	12.2	15.3	4772						CG
NLTT 57749		NLTT 57756	23	10.6	11.3	94.3	3034						CG
NLTT 57823		NLTT 57827	433	10.0	8.8	39.5	23942						CG
NLTT 58235	G273-152	G273-152B	80	5.6	11.3	3.84	430	217.2	10.0	323	0.20	1.000	Z
NLTT 58594		NLTT 58595	388	8.9	8.9	7	3804						CG